PHYSICAL REVIEW B **76**, 125410 (2007)

Surface thermomigration of nanoscale Pt-Si droplets on stepped Si(100)

P. A. Bennett,[1,2,*] J. Chobanian,[1] J. I. Flege,[3] E. Sutter,[3] and P. Sutter[3]
[1]*Department of Physics, Arizona State University, Tempe, Arizona 85287-1504, USA*
[2]*School of Materials, Arizona State University, Tempe, Arizona 85287-8706, USA*
[3]*Center for Functional Nanomaterials, Brookhaven National Laboratory, Upton, New York 11973, USA*

(Received 18 May 2007; revised manuscript received 19 July 2007; published 10 September 2007)

The motion of Pt-Si liquid nanodroplets and their interaction with atomic steps on Si(100) has been studied using low-energy electron microscopy. Submicron droplets migrate across the surface in the direction of the lateral temperature gradient as demonstrated by overlain maps of migration velocity and sample temperature. The thermal migration motion is opposed by a drag force normal to substrate steps, which strongly deflects smaller droplets to move parallel to step edges but hardly affects larger ones. In addition, steps are dragged along by moving droplets before eventually depinning. The resulting curved steps can create "roadways" that collect droplets and guide their motion, resulting in a non-Ostwald coarsening process involving guided collision and coalescence.

DOI: 10.1103/PhysRevB.76.125410 PACS number(s): 68.08.−p, 68.35.Af, 68.37.Nq

I. INTRODUCTION

The behavior of liquid metal nanodroplets on crystalline substrates is a topic of considerable current interest. One important motivation is to better understand the catalyzed growth of nanowires via the vapor-liquid-solid (VLS) mechanism.[1,2] In particular, Si nanowires can be grown by exposing nanometer-sized Au clusters on a Si substrate to silane gas at elevated temperature.[3,4] The Au catalyst, in the form of a Au-Si liquid drop, rides on the end of the growing nanowire and serves as a fast kinetic pathway for Si to leave the gas phase, diffuse through or around the droplet, and condense on the growing Si nanowire. Other material systems behave in a similar fashion.[5] This process depends on the solubility and diffusivity of Si in the liquid eutectic nanodroplet, which are not well known. Indeed, fundamental aspects of liquid eutectics, in general, are poorly understood.[6] Other metals, specifically Pt or Pd, can also be used for VLS nanowire growth, and may have advantages over Au.

The stability and dynamic behavior of nanostructures on solid surfaces are interesting in a broader context as well. For example, intermixing and alloying at surfaces can occur via migration and coalescence of islands of the constituent materials.[7] Another example is contact reactions, in which a film deposited at low temperature is annealed at higher temperature to form a compound with improved crystallinity, conductivity, etc. In such reactions, agglomeration or dewetting of the film at high temperature is carefully avoided.[8] Finally, the process of mass transport between small particles (coarsening) is important in the production of nanoparticle arrays with well defined properties.[9,10]

Thermal migration of droplets or bubbles through solids (rather than on a surface) is a closely related problem that has been studied for many years. Examples include water droplets in limestone, gas bubbles in glass, and voids in metallic interconnects.[11] The fundamental driving force is a lowering of the free energy of the droplet at higher temperature due to entropy of solution. The kinetic mechanism (for an alloy system) involves solution of the matrix into the droplet at the high temperature side, diffusion through or around the droplet, and condensation of matrix material out of the droplet at the low temperature side. For a binary eutectic system, the behavior is particularly interesting, as we show for Pt-Si in Fig. 1. At a typical observing temperature of 1050 °C, the equilibrium phases joined by a $T=1050\ ^\circ\mathrm{C}$ tie line are liquid Au-Si at ∼70% Si and essentially pure Si with a small amount of dissolved Au. Below the eutectic point (980 °C and 67% Si), the two equilibrium phases are solid Pt-Si and pure Si. Cline and Anthony point out that thermomigration in such a system is particularly interesting, since the alloy concentration along the solvus line varies strongly with temperature, leading to very high migration speeds at high temperature where the solvus line flattens out.[12] They show that, within reasonable approximations, the thermal migration speed V for a liquid eutectic droplet can be written as

$$V(T) = \frac{D(T)}{1 - X(T)} \left(\frac{\partial X}{\partial T} \right) \nabla T, \tag{1}$$

where $D(T)$ is the diffusivity of the matrix component in the droplet, $X(T)$ is the normalized alloy fraction along the solvus line, and ∇T is the temperature gradient. In this model,

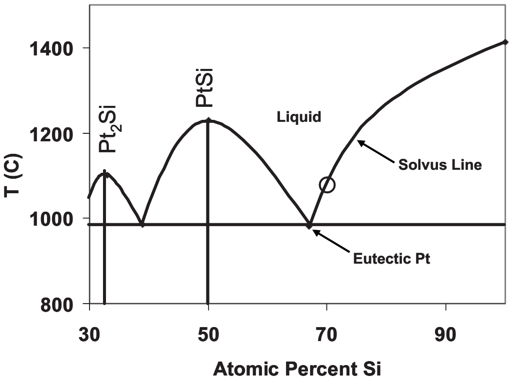

FIG. 1. Si-rich, high temperature portion of the Pt-Si bulk binary phase diagram. The circle marks the expected Pt-Si droplet stoichiometry at $T=1050\ ^\circ\mathrm{C}$.

1098-0121/2007/76(12)/125410(6)

the droplet speed is independent of droplet size since driving force and mobility scale inversely. The thermomigration of liquid Al-Si droplets in bulk silicon is well described by Eq. (1).[12]

There are not many prior studies of the motion of liquid metal droplets on a Si surface. Ichinokawa *et al.* reported that the speed and direction of electromigration of droplets depend on the metal.[13] Liu *et al.* have shown that strain fields can be used to guide the motion of Au-Si liquid droplets on Si(100) bicrystals with buried dislocations.[14] Yang *et al.* have recently studied the motion of micron-sized Pt-Si droplets on Si(100) using photoemission electron microscopy.[15] They obtained a thermal activation energy of 0.57 eV for the diffusivity of Si in the droplet by fitting their data to Eq. (1).

In this paper, we have used primarily low-energy electron microscopy (LEEM) to study the motion of liquid Pt-Si droplets on Si(100). This technique allows video-rate imaging of nanometer-sized droplets at high temperatures. Most importantly, individual atomic steps and their interaction with the moving droplets can be observed. The paper is structured as follows: We discuss first thermal migration and second the effect of step interactions. We find that the thermal migration velocity correlates with thermal gradient in direction and magnitude. The droplet speed is independent of droplet size and varies exponentially with temperature, from which a diffusion constant may be obtained. Dynamic LEEM observations combined with *ex situ* cross-sectional transmission electron microscopy (XTEM) and atomic force microscopy (AFM) suggest that the freezing and melting process is accompanied by a reversible change in stoichiometry of the droplet, as expected from the bulk phase diagram. Substrate steps are found to exert a drag force which can deflect or stop the droplets, with a larger effect on smaller droplets. In addition, step edges are dragged along by moving droplets before eventually depinning. The resulting curved steps can create "roadways" that collect droplets and guide their motion. This results in an unusual coarsening mechanism involving droplet migration and coalescence along one-dimensional pathways. In a related paper, we quantify the drag force from a single step and determine a critical size below which droplets cannot cross the steps.[16]

II. EXPERIMENTAL DETAILS

These experiments were done on an Elmitec LEEM III system in the Center for Functional Nanomaterials at Brookhaven National Laboratory. Si(100) samples (1 Ω cm, *n* type, 0.1° miscut, 10×10 mm^2) were prepared by briefly heating to 1200 °C in UHV to remove oxide and carbon contaminations. Surface cleanliness was verified by the appearance of smooth widely spaced steps in the LEEM image. Pt metal was deposited by sublimation from a high-purity Pt-coated W wire mounted 8 cm from the sample. Coverage was estimated from the volume of spherical droplets observed in the LEEM images. The sample was heated by electron bombardment to the back side with an accelerating voltage of 500–1000 V. Video and still images were acquired with 12 bits resolution. Particle motion was measured using VIDEOPOINT software. At high speed, the moving droplets were blurred due to frame averaging, but their average positions remained well defined. Droplet velocity was measured from 900 to 1130 °C (pyrometer reading). Image drift at high temperature was compensated by subtracting the apparent motion of fixed objects.

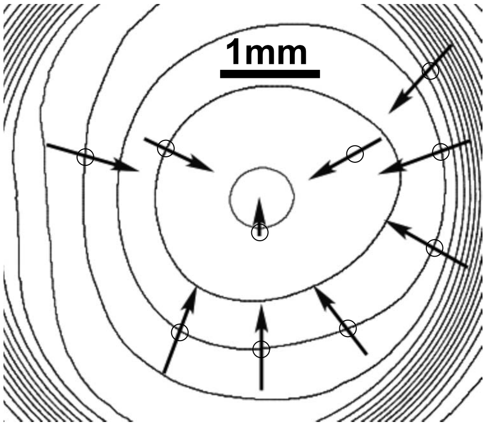

FIG. 2. Contour map of sample temperature with 15 °C spacing between contours and maximum $T=1080$ °C at the center. Arrows indicate the velocity (direction and magnitude) of droplet migration at positions marked by the accompanying small circles (at the center of the arrows).

Sample temperature was determined using a digital optical pyrometer with emissivity $\varepsilon=0.7$ and spot size ~1 mm. This reading represents the hottest portion of the sample, which is near the center. Absolute calibration of temperature is difficult, given the uncertainty of emissivity and window corrections (reflection and absorption). We state everywhere the uncorrected pyrometer readings, consistent with literature practice. We note in passing that the Si sample melted at a pyrometer reading of 1300±40 °C, which compares with the known melting point of $T_{\mathrm{mp,Si}}=1412$ °C. We found that the measured melting point for droplets of Pt-Si was $T\sim885\pm20$ °C. This compares with $T_0=980$ °C for the most Si-rich eutectic at 67% Si. We believe that the apparent difference in both cases is due to pyrometer corrections for emissivity and window effects. That is, the Pt-Si islands actually melt at 980 °C. The temperature profile across the surface was determined from a three-color digital photograph of the glowing sample. Image brightness vs temperature was calibrated by matching the brightness at the sample center with the optical pyrometer reading for a series of heating power values.

III. RESULTS AND DISCUSSION

A. Temperature dependence of motion

We begin with a discussion of the temperature dependence of droplet migration, ignoring step interactions for the moment. The first feature to explore is the dependence of velocity on temperature gradient. The temperature gradient arises through inhomogeneous heating of the sample during electron bombardment to the back side. The resulting temperature profile is shown as a contour map in Fig. 2. The outer rim of the sample is ~200 °C cooler than the center due to the filament geometry and conductive heat loss at the

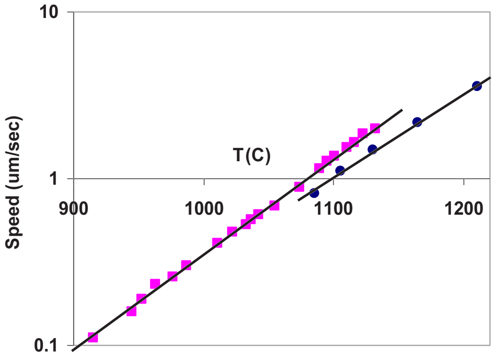

FIG. 3. (Color online) Speed vs temperature for droplet migration, measured at a single location on the surface (squares). Data from Ref. 15 are also shown (circles). Trend lines are only guides for the eye.

edges of the holder. The figure also shows the migration velocity (speed and direction) for droplets at various locations on the sample. These data were taken by recording a video sequence at a given location, translating the sample ~1 mm, realigning the microscope, and then recording another video sequence. Droplet velocity was determined offline by tracking the motion of a few droplets as they passed through the field of view. The peak temperature near the sample center remained fixed at $T=1080$ °C for the entire set of map measurements.

Visual inspection of the combined plot shows that the speed and direction of droplet motion is roughly proportional to the direction and magnitude of the temperature gradient. In particular, the migration direction spans almost a full circle, while the speed is nearly zero at the center, where the temperature gradient is small. Observations more than 2 mm from the center could not be made due to difficulty in aligning the microscope in that case. Overall, it is clear that the droplets move toward the highest temperature and, therefore, collect near the sample center.

Next we explore the variation of migration speed with absolute temperature. This is shown in Fig. 3. These measurements were made at a location ~2 mm from the sample center, where the direction of the temperature gradient is well defined. We estimate that the magnitude of the gradient changes in proportion to the value of temperature. A video sequence was recorded while the temperature was continuously ramped from 900 to 1150 °C. The droplets ranged in size from 0.5 to 1.0 μm, but showed no difference in speed at a given temperature. The data are plotted on a semilogarithmic scale to better show the dynamic range and the exponential trend. The uncertainty in each speed value is implied by the deviation from the trend line. Data from Yang *et al.* are included as well and follow the same trend as our data. The small offset between the data sets is believed to be due to temperature calibration between the two experiments, and is not significant in this context.

Following the model of Eq. (1), these data may be used to extract $D(T)$, the temperature-dependent diffusivity of silicon through the Pt-Si droplet, assuming volume diffusion and equilibrium values for the solvus line, $X(T)$. Yang *et al.* have made this analysis and obtained $D(T)=D_0\exp(-Q/kT)$, where $D_0=(5.5\pm0.2)\times10^{-2}$ cm^2 s^{-1} and $Q=0.57\pm0.06$ eV. Our data for $v(T)$ closely match those of Yang *et al.*, hence, we do not repeat the analysis here. We note, however, that unlike Yang *et al.*, we find that $v(T)$ remains finite all the way down to the freezing point, where it drops to zero abruptly.

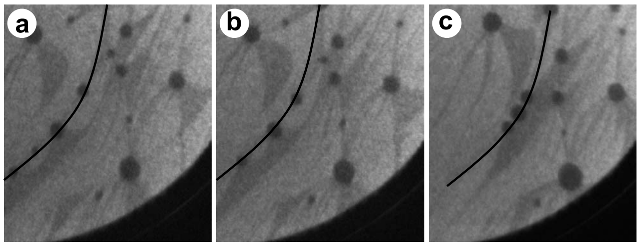

FIG. 4. Coarsening sequence at 950 °C [4.2 eV, 3 μm field of view (FOV)]. The line traces a step bunch, along which some of the droplets move and coalesce by collision. Elapsed times are 0, 25, and 70 s for frames (a), (b), and (c), respectively.

B. Influence of steps

Next we discuss the effect of steps on the motion of droplets and vice versa. Figure 4 shows the motion of very small droplets during the early stage of coarsening. Approximately 10 ML of Pt were deposited at room temperature and then annealed at 950 °C while recording the motion with LEEM. The film has melted and broken into liquid, spherical droplets ranging in diameter from 50 to 250 nm. During the time span of 70 s, the droplets coarsen by moving along step edges (or step bunches) and merging. Isolated droplets do not change size. A line drawn in the figure indicates one step bunch, along which several droplets are seen to move. The black and white terrace contrast corresponds to alternate regions of 2×1 and 1×2 reconstructions of the Si(100) surface, which are necessarily separated by an odd number of single-atom steps.[17]

The melting process was observed directly, as shown in Fig. 5. At $T=885$ °C [Fig. 5(a)], the island had just begun to melt. It displayed rounded corners and flat facetted sides with fourfold symmetry. The center of the island was changing quickly and appeared to be fluid. There was no net motion of the island at this point. In Fig. 5(b), the island had melted completely at a pyrometer reading of 920 °C, corresponding to a true temperature of $T=980$ °C, matching the known bulk eutectic temperature. The black and white terrace contrast at the original location of the island indicates a crater that quickly filled in and flattened when the droplet began to move. The crater may be due to the extension of the solid Pt-Si island into the surface. Such "endotaxial" structures are common for silicide islands.[18] Alternatively, the crater may be formed or altered during the melting process. This follows from the binary phase diagram, which is shown in Fig. 1. At the eutectic temperature, the solid phase is 50% Si (i.e., stoichiometric Pt-Si), while the liquid state is 67% Si. Passing through the eutectic point then requires the incorporation of 17% more Si into the droplet. The appearance of a crater upon melting is consistent with this picture. Conversely, cooling through the eutectic point requires expulsion

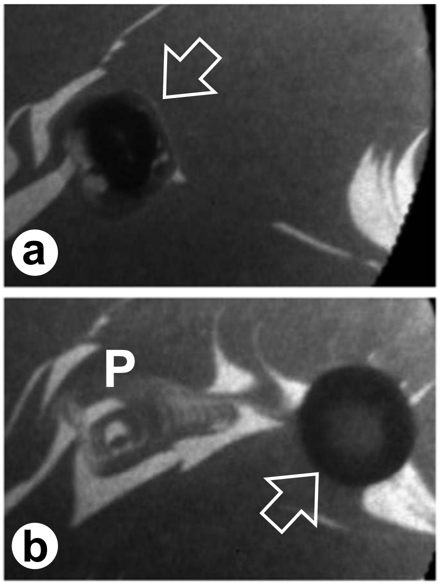

FIG. 5. Melting of Pt-Si island (marked by arrows) and subsequent motion (2.5×3 μm FOV). (a) At $T=885$ °C, the island is solid and facetted. (b) At $T=920$ °C, the island is molten, round, and moving. P marks a crater left behind.

of 17% Si, which would appear as a pedestal under the droplet. Such a pedestal would not be directly visible in LEEM due to the normal incidence, but is suggested by XTEM and AFM images obtained after cooling to room temperature, as presented in Fig. 6. The transmission electron microscope image [Fig. 6(a)] clearly shows a Si pedestal directly under the Pt-Si island after quenching the sample temperature below the melting point. If, however, the sample is cooled slowly, it expels silicon while still moving, leaving a trailing ridge. This phenomenon is suggested by the AFM image in Fig. 6(b). The curvature of the paths is supposed due to deflection by step bunches.

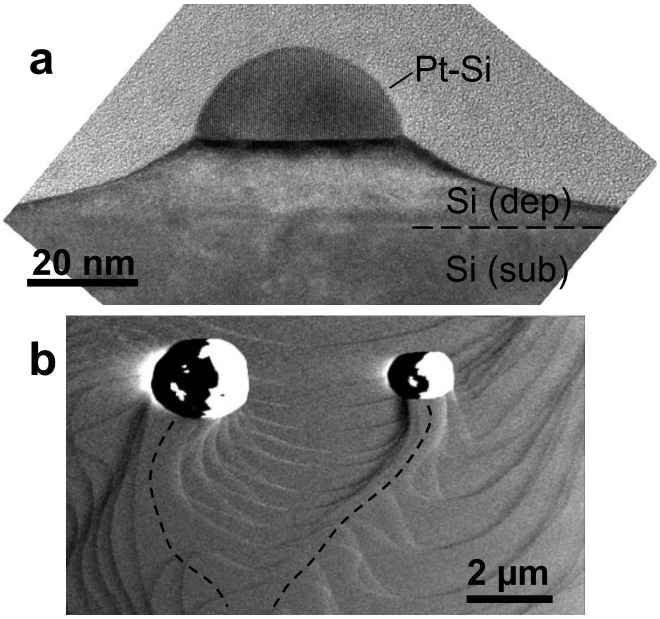

FIG. 6. (a) Cross-sectional transmission electron micrograph of a Pt-Si particle following quench cooling. (b) Derivative mode AFM image following slow cooling, which shows Si ridges in the wake of the particles.

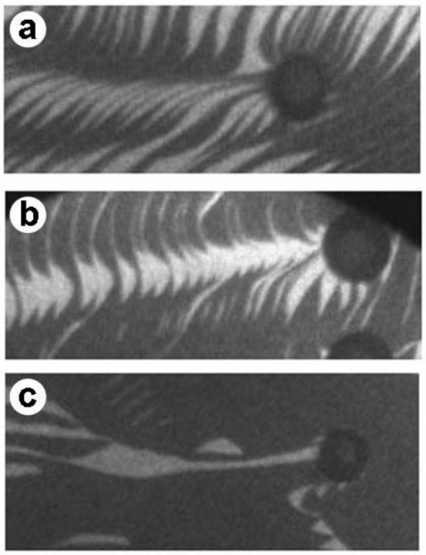

FIG. 7. Step pattern left behind by moving droplets: (a) $T=980$ °C, (b) $T=910$ °C, (c) $T=890$ °C (2.3 eV, 4 μm FOV).

The moving droplets also affect the step edges as they cross over them. This is demonstrated in Fig. 7, which shows the step pattern created by moving droplets at three different temperatures. It is apparent that the step is dragged along for awhile as the droplet crosses over it. These images show step-up motion, but the same behavior occurs for step-down motion. These directions are distinguished by noting the motion of steps during sublimation at high temperature. The step eventually depins from the moving droplet and (partially) straightens out, driven by the intrinsic line tension of the step.[19,20] We emphasize that there is no net exchange of Si or Pt with the droplet during the step crossing. Indeed, droplets show no change in size during tens of minutes and tens of microns of motion. The change in step length, of course, requires exchange of Si adatoms with the terraces. At high temperature [Fig. 7(a), $T=980$ °C], the initial deformation after depinning is small and heals quickly, leaving little net change. At middle temperature [Fig. 7(b), $T=910$ °C], the step deformation is more pronounced and lasts longer. At low temperature [Fig. 7(c), $T=890$ °C], the steps remain pinned and do not straighten at all on this time scale.

The step-straightening process is shown dramatically in Fig. 8. Here, we can see the path of a droplet that has crossed several widely separated steps at nearly right angles. The leading step is still pinned to the droplet and has been pulled very far along, while other steps further back along the path have depinned and have relaxed in proportion to the time (distance traveled) since depinning. This figure also shows clearly that the droplet motion is not somehow *caused* by the steps, since it continues in the center of very wide terraces far from any steps.

The step-deformation process can lead to interesting, dramatic effects, as shown in Fig. 9. This shows the step pattern generated after 30 min of droplet motion at $T=1100$ °C. The

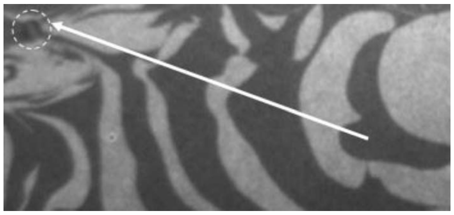

FIG. 8. Step pattern left behind a single moving droplet at $T = 1100\ ^\circ\mathrm{C}$. The arrow indicates the path of motion, but is drawn slightly offset to avoid obscuring the path (1.7 eV, 25 μm FOV).

temperature gradient is nearly vertical (down) in this figure. The local step-down direction is nearly parallel to this, by coincidence. Large droplets follow the direction of the thermal gradient (down), but most droplets follow the slanted roadway instead. This roadway comprises a dense bunch of steps that arise from a positive feedback mechanism as follows: The direction of droplet motion is determined by a competition between the thermal gradient force and the drag force as droplets cross over steps. The droplets pull and distort the steps as they cross over. Subsequent droplets tend to follow the distorted step, veering toward the maximum curvature point and further stretching the step as they cross over.

The road building process can be seen in Fig. 9. Thus, in Fig. 9(a), droplets 2 and 3 are on the roadway and stay on it as they move. The roadway meanders on a path that is distinctly away from both the thermal gradient and the "downhill" gradient of nearby steps. Droplet 1 is traveling off the roadway, moving parallel to the thermal gradient, and crossing individual steps at nearly right angles. The step structure behind this droplet displays a subsidiary roadway that will gradually build up as further droplets follow that path. In Fig. 9(b), droplet 1 climbs onto the main roadway (ascending a step bunch parallel to the roadway) and then collides and merges with droplet 2 on the roadway. The combined droplets (1 and 2) move down the main roadway at roughly the same speed as droplet 3 moving ahead of it. In Fig. 9(d), a large droplet is traveling down the subsidiary roadway started by droplet 1. It climbs up, over and down the main roadway, and continues building a subsidiary roadway. The directions of these two roadways are distinctly different. This is indirectly due to the coarsening process: The main roadway was established early on by small droplets that established some compromise direction between step edges and temperature gradient. At later times, most droplets have grown larger by collision and merging. Hence, they follow the thermal gradient, even if that crosses an existing roadway.

These step effects lead to an unusual coarsening process. In classic Ostwald ripening, mass transport between islands occurs via isolated atoms or molecules and is driven by a variation of chemical potential with size. In the present case, there is no mass transport between isolated Pt-Si droplets. This is consistent with the vapor pressure of Pt, which is $P_{\mathrm{vp}} < 10^{-10}$ Torr at 1100 °C. Droplets change size only by collision and coalescence. In the absence of step interactions, Pt-Si droplets would not coarsen because the migration paths of nearby droplets are essentially parallel. In this sense, steps cause or facilitate the coarsening process. On the other hand, the rearrangement of steps creates a network of one-dimensional paths, which tends to inhibit collisions. This effect is counterbalanced by the redirection of (smaller) droplets onto the roadways.

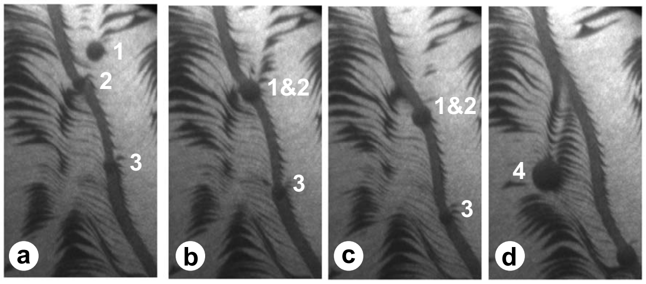

FIG. 9. Image sequence showing a "roadway" built up by multiple passes of droplets at $T = 1100\ ^\circ\mathrm{C}$ ($5 \times 10\ \mu\mathrm{m}$ each panel). Droplets of interest are numbered. Elapsed times are 0, 5, 10, and 30 s for panels (a)–(d), respectively.

IV. SUMMARY AND CONCLUSION

We have shown with dynamical LEEM observations that nanometer-sized Pt-Si liquid droplets move in the direction of higher temperature via a thermal migration mechanism. Their speed is independent of size and varies exponentially with temperature, beginning at the bulk eutectic melting point. The droplets experience a retarding force while crossing steps, which deflects them parallel to the step edge. The couplet reaction force on the step causes it to stretch out before eventually depinning. The net effect is to create narrow roadways of step bunches that guide the motion of following droplets. Droplets do not change size during migration, except by guided collision and merging with other droplets, which comprises a non-Ostwald coarsening process.

The thermomigration motion of Pt-Si liquid droplets on a Si surface is a complex mixture of the factors described in the paper. This interesting phenomenon will certainly apply to other material systems. In a practical context, it may provide a means for manipulating the self-assembly process for nanostructure arrays. For example, a patterned array of depressions or mounds might be used to guide droplets into a regular array via step steering mechanism. Alternatively, droplet coalescence might usefully be suppressed on a regular step array since droplet motion would be largely parallel to the steps.

ACKNOWLEDGMENTS

We gratefully acknowledge the support of NSF NIRT Grant No. ECS-0304682. The use of the facilities within the Center for Solid State Science at Arizona State University and facilities in the Center for Functional Nanomaterials, under the auspices of the U.S. Department of Energy, was made possible through Contract No. DE-AC02-98CH1-886.

*peter.bennett@asu.edu

[1] R. S. Wagner and W. C. Ellis, Appl. Phys. Lett. **4**, 89 (1964).

[2] E. I. Givargizov, J. Cryst. Growth **31**, 20 (1975).

[3] J. B. Hannon, S. Kodambaka, F. M. Ross, and R. M. Tromp, Nature (London), **440**, 69 (2006).

[4] Y. Homma, P. Finnie, and T. Ogino, Appl. Phys. Lett. **74**, 815 (1999).

[5] P. Yang, MRS Bull. **30**, 85 (2005).

[6] B. Bokhonov and M. Korchagin, J. Alloys Compd. **312**, 238 (2000).

[7] A. K. Schmid, N. C. Bartelt, and R. Q. Hwang, Science **290**, 1561 (2000).

[8] A. H. Reader, A. H. von Ommen, P. J. W. Weijs, R. A. M. Wolters, and D. J. Oostra, Rep. Prog. Phys. **56**, 1397 (1993).

[9] J. A. Floro, E. Chason, M. B. Sinclair, L. B. Freund, and G. A. Lucadamo, Appl. Phys. Lett. **73**, 951 (1998).

[10] V. A. Shchukin, N. N. Ledentsov, P. S. Kopev, and D. Bimberg, Phys. Rev. Lett. **75**, 2968 (1995).

[11] T. R. Anthony and H. E. Cline, J. Appl. Phys. **42**, 3380 (1971).

[12] H. E. Cline and T. R. Anthony, J. Appl. Phys. **47**, 2325 (1976).

[13] T. Ichinokawa, H. Izumi, C. Haginoya, and H. Itoh, Phys. Rev. B **47**, 9654 (1993).

[14] C. H. Liu, W. W. Wu, and L. J. Chen, Appl. Phys. Lett. **88**, 133112 (2006).

[15] W. C. Yang, H. Ade, and R. J. Nemanich, Phys. Rev. B **69**, 045421 (2004).

[16] P. Sutter, P. A. Bennett, J. I. Flege, and E. Sutter, Phys. Rev. Lett. (to be published).

[17] P. Sutter and M. G. Lagally, Phys. Rev. Lett. **82**, 1490 (1999).

[18] Z. He, D. J. Smith, and P. A. Bennett, Phys. Rev. Lett. **93**, 256102 (2004).

[19] N. C. Bartelt and R. M. Tromp, Phys. Rev. B **54**, 11731 (1996).

[20] R. M. Tromp and J. B. Hannon, Surf. Rev. Lett. **9**, 1565 (2002).